

# Object detection via a multi-region & semantic segmentation-aware CNN model

Spyros Gidaris

Universite Paris Est, Ecole des Ponts ParisTech

gidariss@imagine.enpc.fr

Nikos Komodakis

Universite Paris Est, Ecole des Ponts ParisTech

nikos.komodakis@enpc.fr

## Abstract

We propose an object detection system that relies on a multi-region deep convolutional neural network (CNN) that also encodes semantic segmentation-aware features. The resulting CNN-based representation aims at capturing a diverse set of discriminative appearance factors and exhibits localization sensitivity that is essential for accurate object localization. We exploit the above properties of our recognition module by integrating it on an iterative localization mechanism that alternates between scoring a box proposal and refining its location with a deep CNN regression model. Thanks to the efficient use of our modules, we detect objects with very high localization accuracy. On the detection challenges of PASCAL VOC2007 and PASCAL VOC2012 we achieve mAP of 74.9% and 70.7% correspondingly, surpassing any other published work by a significant margin.

## 1. Introduction

One of the most studied problems of computer vision is that of object detection: given an image return all the instances of one or more type of objects in form of bounding boxes that tightly enclose them. The last two years, huge improvements have been observed on this task thanks to the recent advances of deep learning community [18, 2, 14]. Among them, most notable is the work of Sermanet et al. [23] with the Overfeat framework and the work of Girshick et al. [10] with the R-CNN framework.

Overfeat [23] uses two CNN models that applies on a sliding window fashion on multiple scales of an image. The first is used to classify if a window contains an object and the second to predict the true bounding box location of the object. At the end, the dense class and location predictions are merged with a greedy algorithm in order to produce the final set of object detections.

R-CNN [10] uses Alex Krizhevsky’s Net [17] to extract features from box proposals provided by selective search [26] and then classifies them with class specific linear SVMs. They manage to train networks with millions



**Figure 1:** **Left:** detecting the sheep on this scene is very difficult without referring on the context, mountainish landscape. **Center:** In contrast, the context on the right image can only confuse the detection of the boat. The pure object characteristics is what a recognition model should focus on in this case. **Right:** This car instance is occluded on its right part and the recognition model should focus on the left in order to confidently detect.

of parameters by first pre-training on the auxiliary task of image classification and then fine-tuning on a small set of images annotated for the detection task. With this simple pipeline, they managed to surpass by a large margin the detection performance of all the previous art on the field that includes complex methods such as deformable parts models [9] or the non-linear multi-kernel approach of [27]. Their success comes from the fact that they replaced the hand-engineered features like HOG [4] or SIFT [21] with the high level object representations produced from the last layer of a CNN model. By employing an even deeper CNN model, such as the 16-layers VGG-Net [24], they boosted the performance another 7 points.

The lesson learned is that indeed features matter a lot on object detection and our work is partly motivated from this observation. However, instead of proposing a deeper architecture, here we opt for an architecture that is wider, *i.e.*, one whose last hidden layers provide features of increased dimensionality. This is accomplished in two levels:

1. On the one hand, we build a rich candidate box representation that captures several different aspects of an object such as its pure appearance characteristics, the joint appearance on both sides of the object borders, the distinct appearance of its different regions, context appearance, and semantics. We believe that such a rich representation will facilitate the problem of recognising difficult object instances under a variety

of circumstances like those depicted in figure 1. In order to achieve our goal, we propose a multi-component CNN model, called multi-region CNN hereafter, each component of which is steered to focus on a different region of the object thus enforcing diversification of the discriminative appearance factors captured by it. Furthermore, as we will explain, by properly choosing and arranging some of these regions, our goal is also to help our representation in being less invariant to inaccurate localization of an object (note that this property, which is highly desirable for detection, contradicts with the built-in invariances of CNN models, which stem from the use of max-pooling layers).

2. On the other hand, we also enrich the above representation through novel CNN-based semantic segmentation-aware features, trained without requiring any object segmentation annotations. In this manner, we also show that taking into account semantic-segmentation information helps also for the detection task.

We are also motivated from the observation that, due to the tremendous classification capability of the recent CNN models [17, 24, 16, 13, 25], the bottleneck for good detection performance is now the accurate object localization. Indeed, it was noticed on R-CNN [10] that the most common type of false positives is the mis-localized detections. They fix some of them by employing a post processing step of bounding box regression that they apply on the final list of detections. However, their technique only helps on small localization errors. We believe that there is much more space for improvement on this aspect. In order to prove it, we attempt to built a more powerful localization system that relies on combining our multi-region CNN model with a CNN-model for bounding box regression, which are used within an iterative scheme that alternates between scoring candidate boxes and refining their coordinates.

Our contributions are:

- We develop a multi-region and semantic segmentation-aware CNN recognition model that yields an enriched object representation capable to capture a diversity of discriminative appearance factors and to exhibit localization sensitivity that is desired for the task of accurate object localization.
- We show how to significantly improve the localization capability by coupling the aforementioned CNN recognition model with a CNN model for bounding box regression, adopting a scheme that alternates between scoring candidate boxes and refining their locations, as well as modifying the post-processing step of non-maximum-suppression.

- Our detection system achieves mAP of 74.9% and 70.7% on VOC2007 [7] and VOC2012 [8] detection challenges respectively, thus surpassing the previous state-of-art by a very significant margin.

## 2. Multi-Region CNN Model

The recognition model that we propose consists of a multi-component CNN network, each component of which is chosen so as to focus on a different region of an object. As already explained, one of the goals of using such a network is to capture various complementary aspects of the object’s appearance. We call this a Multi-Region CNN model.

The overall architecture of such a model can be seen in figure 2. Initially, the entire image is forwarded through the convolutional layers of the model and the activation maps are produced. This part of the network is called the activation-maps module. Then a candidate detection box  $B$  is analysed on a set of overlapping regions  $\{R_i\}_{i=1}^k$ , which are projected on the activation maps (note that these regions are always defined relatively to the bounding box  $B$ ). The activations that lay inside them are cropped, pooled with spatially adaptive max-pooling layers [12], and forwarded through region dedicated multi-layer networks. Each such region-subnetwork is called a region-adaptation module. Finally, the candidate box representation is obtained by concatenating the last hidden layer outputs of all the region sub-networks. We note that we utilize 2 types of shapes for the regions: rectangles and rectangular rings (where the latter is defined in terms of an inner and outer rectangle).

When designing the architecture of the Multi-Region CNN model, we came across the dilemma if we should project each region on the pixel domain or on the last convolutional layer domain. The reason for finally choosing the latter option was made mainly for computational reasons, since projecting all the different regions on pixel level and forwarding them through a CNN would considerably increase the computational time both during training and testing. For instance, the 16-layer deep VGG model [24], which when used in the R-CNN [10] framework gives state-of-the-art results, has runtime of 1 minute for testing 2000 candidate boxes. Multiplying this time by the number of our regions would render the model much less efficient. Instead, we decided to adopt for our Multi-Region CNN model the SPP-Net object detection paradigm [12]. This way, the computation needed for applying the convolutional layers on all the regions and for all the candidate detection boxes inside an image is shared. Regarding the regions that are rectangular rings, both the inner and outer box are projected on the activation maps of the last convolutional layer and then the activations that lay inside the inner box are masked out by setting them to zero. This processing step is similar to the Convolutional Feature Masking layer proposed on [3] in order to mask segment proposals ([26, 1]) for the task

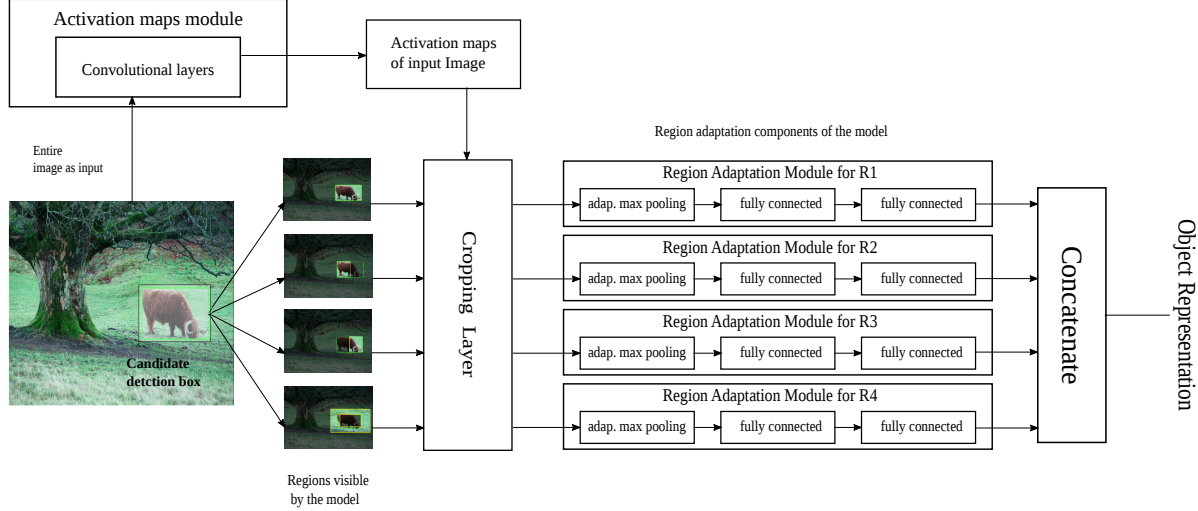


**Figure 2:** Multi Region CNN architecture. For clarity we present only four of the regions that participate on the initial Multi-Region CNN architecture. An “adaptive max pooling” layer uses spatially adaptive pooling as in [12] (but with a one-level pyramid).

of object segmentation.

To conclude, the architecture of the Multi-Region CNN model that we just described, is composed of:

**The activation maps module.** Extracts convolutional feature maps from the entire image. Its architecture is consisted of the convolutional part of the 16-layers VGG-Net [24] that outputs feature maps of 512 channels. The max-pooling layer right after the last convolutional layer is omitted on this module.

**The region adaptation modules**  $\{R_i\}_{i=1}^k$ . Given a candidate detection box and the activation maps of the image, each of them extracts a high level feature from its assigned region. They are consisted of a spatially adaptive max-pooling layer [12] that outputs fixed size features of 512 channels on a  $7 \times 7$  grid, and the two fully connected layers of VGG-Net [24] that have 4096 output channels each.

Despite the specific architecture choices that we made till now, the activation maps module followed by region adaptation modules, is a general architecture abstraction that can be easily adjusted, as we will see, in other realizations.

## 2.1. Region components and their role on detection

Here we describe the regions included on the Multi-Region CNN model and discuss their role on object detection.

**Original candidate box:** this is the candidate detection box itself as being used on R-CNN [10] (figure 3a). A network trained on this type of region is guided to capture the appearance information of the entire object. When this region is used alone consists the baseline of our work.

**Half boxes:** those are the left/right/up/bottom half parts of a candidate detection box (figures 3b, 3c, 3d, 3e). Net-

works trained on each of those regions are guided to learn the appearance characteristics present only on each half part of an object or on each side of the objects borders, aiming also to make the representation more robust with respect to occlusions.

**Central Regions:** there are two type of central regions included in our model. The first is the box obtained by shrinking the candidate box by a factor of 0.5 (figure 3f). The second one is a rectangular ring where the inner box is obtained by shrinking the candidate box by a factor of 0.3 and the outer box by shrinking it by 0.8 (figure 3g). The networks trained on them are guided to capture the pure appearance characteristics of the central part of an object which is probably less interfered from other objects next to it or its background.

**Border Regions:** in our model we include two regions dedicated to focus their attention on the borders of an object. Those regions have the form of rectangular rings. For the first region, we obtain the inner box by shrinking the candidate box by a factor of 0.5 while the outer box has the same size as the candidate box (figure 3h). For the second region, its inner box is obtained by shrinking the candidate box by a factor of 0.8 and the outer box is obtained by enlarging the candidate box by a factor of 1.5 (figure 3i). With those regions, we expect to guide the dedicated on them networks to focus on the joint appearance characteristics on both sides of the object borders, also aiming to make the representation more sensitive to inaccurate localization.

**Contextual Region:** this is again a rectangular ring where its inner box is the candidate box itself and the outer box is obtained by enlarging the candidate box by a factor of 1.8 (figure 3j). The network dedicated on this region is driven to focus on the contextual appearance that surrounds

an object such as the appearance of its background or of other objects next to it.

Concerning the general role of the regions on object detection, we briefly focus below on two of the reasons why they are helpful on this task:

*Discriminative feature diversification.* Our hypothesis is that having regions that render visible to their network-components only a limited part of the object or only its immediate surrounding forces each network-component to discriminate image boxes solely based on the visual information that is apparent on them thus diversifying the discriminative factors captured by our overall recognition model. For example, if the border region depicted on figure 3i is replaced with one that includes its whole inner content, then we would expect that the network-component dedicated to it will not pay the desired attention on the visual content that is concentrated around the borders of an object. We tested such a hypothesis by conducting an experiment where we trained and tested two Multi-Region CNN models consisted of two regions each. Model A included the original box region and the border region depicted on figure 3i that does not contain the central part of the object. On model B, we replaced the rectangular ring with a normal box of the same size as the outer box on the rectangular ring on figure 3i. Both of them were trained on PASCAL VOC2007 [7] trainval set and tested on the test set of the same challenge. Model A achieved 64.1% mAP while Model B achieved 62.9% mAP which is 1.2 points lower and validates our assumption.

*Localization-aware representation.* Moreover, we argue that the multi-region architecture of our model as well as the type of regions included address to a certain extent one of the major problems on the detection task, which is the inaccurate localization of object instances. We expect that having multiple regions with network-components dedicated on each of them, imposes soft constraints regarding the visual content allowed on each type of region for a given candidate detection box. We provide experimental support for this argument by referring to sections 6.2 and 6.3.

### 3. Semantic Segmentation-Aware CNN Features

To further diversify the features encoded by our representation, we extend the Multi-Region CNN model so that it can also incorporate semantic segmentation-aware CNN features (see figure 4). We were motivated for this also from the close connection between segmentation and detection, and the fact that segmentation related cues have been empirically known to help object detection [6, 11, 22]. In the context of our multi-region CNN network, the incorporation of the semantic segmentation-aware features is done by properly adapting the two main modules of the network, *i.e.*, the *activation-maps module* and the *region-adaptation*



**Figure 3:** Illustration of the regions components used.

*modules* (see architecture in figure 4). We hereafter refer to the resulting modules as:

- *Activation maps module for semantic segmentation-aware features.*
- *Region adaptation module for semantic segmentation-aware features.*

It is important to note that the modules for the semantic segmentation-aware features are trained *without the use of*

any additional annotation. Instead, they are trained in a *weakly supervised manner* using only the provided bounding box annotations for detection.

We combine the initial Multi-Region CNN model with the semantic segmentation aware CNN model by simply concatenating the outputs of their last hidden layers (see figure 4).

### 3.1. Activation Maps Module for Semantic Segmentation-Aware features

**Fully Convolutional Nets.** Our semantic segmentation aware activation maps module has the architecture of a Fully Convolutional Net [20], abbreviated hereafter as FCN (we refer the interested reader to [20] for more details about FCN where it is being used for the task of semantic segmentation). In our work, we use as FCN the 16-layers VGG-Net [24] by reshaping its last three fully connected layers ( $fc_6$ ,  $fc_7$ , and  $fc_8$ ) to convolutional ones of kernel size  $7 \times 7$ ,  $1 \times 1$ , and  $1 \times 1$  correspondingly. The last – classification – layer of our FCN outputs as many channels as our classes.

**Feature dimensionality reduction of the activation maps.** Furthermore, in order to be able to efficiently store the activation maps of an image on the hard disk, we reduce the dimensionality of the last hidden layer,  $fc_7$ , from 4096 channels to 512 channels. To accomplish that, after the fine-tuning of the FCN with 4096 channels on the  $fc_7$  layer has converged, we replace the  $fc_7$  layer with another one that has 512 output channels and is initialized from a Gaussian distribution. Then, the training of the FCN starts from the beginning and is continued until convergence again. Finally, for the activation maps module of the semantic segmentation-aware CNN, the new FCN with the 512 output channels is used.

**Weakly Supervised Training.** To train the activation maps module for the class-specific foreground segmentation task, we only use the annotations provided on object detection challenges (so as to make the training of our overall system independent of the availability of segmentation annotations). To that end, we follow a weakly supervised training strategy and we create artificial foreground class-specific segmentation masks using bounding box annotations. More specifically, the ground truth bounding boxes of an image are projected on the spatial domain of the last hidden layer,  $fc_7$ , and the cells that lay inside the projected boxes are labelled as foreground while the rest are labelled as background (see left and middle column in figure 5). The aforementioned process is performed independently for each class and yields as many segmentation masks as the number of our classes. As can be seen in figure 5, despite the weakly supervised way of training, the resulting activations carry significant semantic segmentation information, enough even to delineate the boundaries of the object and

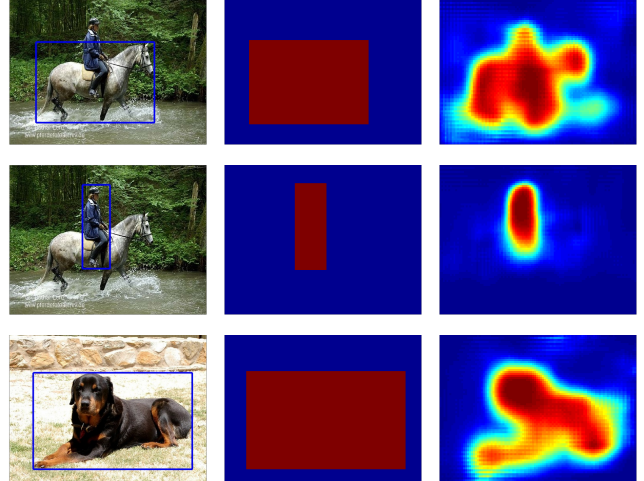


**Figure 5:** **Left column:** images with the ground truth bounding boxes drawn on them. The classes depicted from top to down order are horse, human, and dog. **Middle column:** the segmentation masks artificially generated from the ground truth bounding box on the left column. We use blue color for the background and red color for the foreground. **Right column:** the foreground probabilities estimated from our trained FCN model. These clearly verify that, despite the weakly supervised training, our extracted features carry significant semantic segmentation information.

separate the object from its background.

### 3.2. Region Adaptation Module for Semantic Segmentation-Aware Features

After the FCN has been trained on the auxiliary task of foreground segmentation, we drop the last classification layer and we use the rest of the FCN network in order to extract from images semantic segmentation aware activation maps. We exploit those activation maps by treating them as mid-level features and adding on top of them a single region adaptation module trained for our primary task of object detection.

**Architecture.** The architecture of our adaptation module consists of *a*) a spatially adaptive max-pooling layer [20] that outputs feature maps of 512 channels on a  $9 \times 9$  grid, and *b*) a fully connected layer with 2096 channels.

**Single Region Choice.** For the semantic segmentation-aware CNN extension, we chose to use only one region obtained by enlarging the candidate detection box by a factor of 1.5 (such a region contains semantic information also from the surrounding of a candidate detection box). The reason that we did not repeat the same regions that were used on the initial Multi-Region CNN architecture is for efficiency as these are already used for capturing the appearance cues of an object.

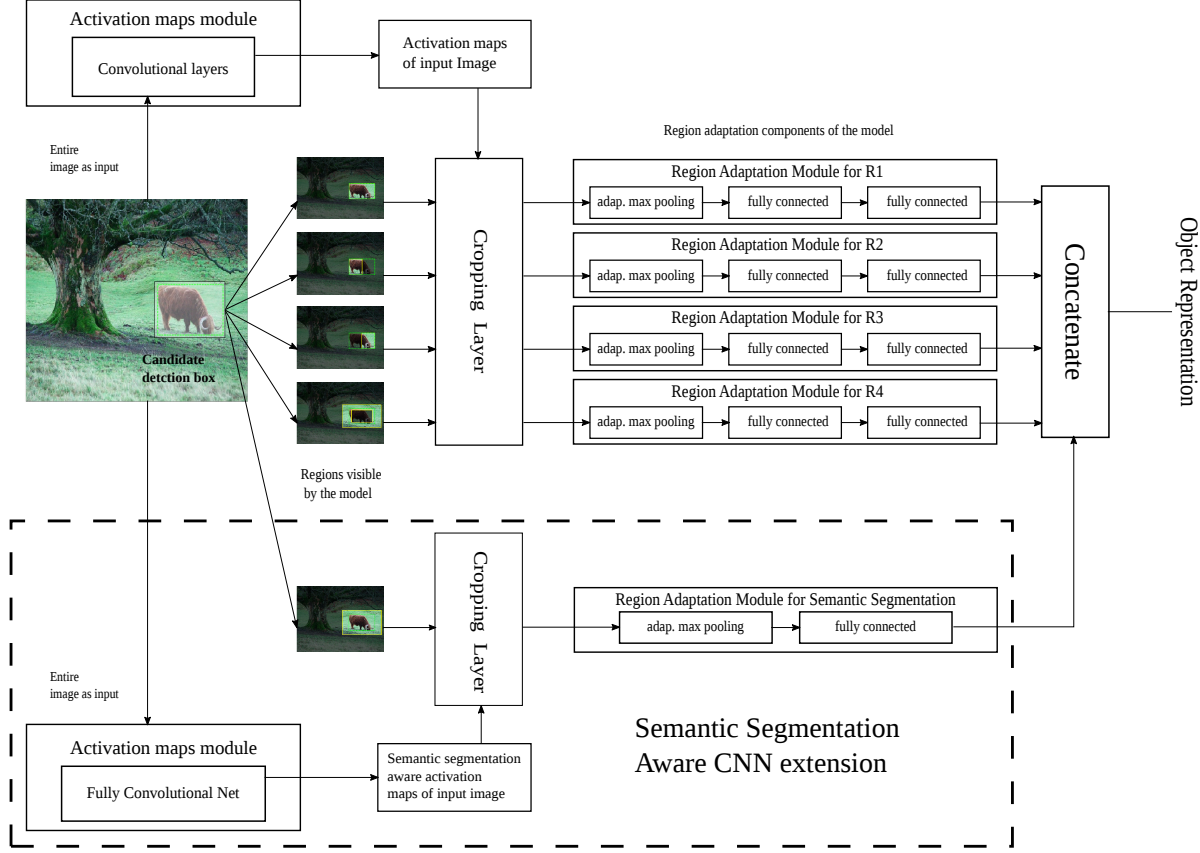


**Figure 4:** Multi Region CNN architecture extended with the semantic segmentation-aware CNN features.

## 4. Object Localization

As we already explained, our Multi-Region CNN based recognition model exhibits the localization awareness property that is necessary for accurate object localization. However, by itself it is not enough. In order to make full use of it, our recognition model needs to be presented with well localized candidate boxes that in turn will be scored with high confidence from it. However, the selective search algorithm that we use, proposes category independent box proposals that cover with high recall the objects of an image but without having them localized accurately enough. A different way to proceed would be to use our recognition model on a sliding window fashion and on multiple scales and aspect ratios in an image but that would be a computationally expensive solution. Instead the solution that we adopt is:

- **CNN-based regression.** We introduce an extra multi-layer region sub-network that, instead of being used for object recognition, is trained to predict the actual object location. This bounding box regression region module, is applied on top of the activation maps produced from the initial Multi-Region CNN model and is consisted of two hidden fully connected layers with

4096 channels each (as the fully connected layers of VGG-Net) and a regression layer that predicts  $4 \times C$  values where  $C$  is the number of categories. In order to allow it to predict the location of object instances that are not in the close proximity of any of the initial candidate boxes, we use as region a box obtained by enlarging the initial candidate box by a factor of 1.3.

- **Iterative Localization:** we use an iterative scheme that alternates between scoring a set of proposals with our recognition model and refining their locations with the CNN-based bounding box regression. With this scheme, we obtain candidate boxes that both exhibit high recall of the objects on an image and are well localized on them. We found out that two iterations of our scheme are enough for convergence. For the first iteration, the box proposals are coming from selective search algorithm [26]. After being scored, those with very low confidence are rejected in order to reduce the computational burden of the subsequent iteration(s).
- **Bounding box voting.** After the last iteration of our iterative scheme, the scored boxes produced on each step are merged together. Because of the multiple re-

gression steps, the generated boxes will be highly concentrated around the actual objects of interest. We exploit this "by-product" of the iterative localization scheme by modifying the non-maximum-suppression step that is performed at post-process time. Specifically, after peaking the box with the highest score on its neighbourhood, we predict the final object location by having each of the boxes that overlap with the peaked one by more than 0.5 (on IoU) to vote for the bounding box location using its score as weight.

In figure 6 we provide a visual illustration of the object localization.

## 5. Implementation details

For all the CNN models involved in our proposed system, we used the publicly available 16-layers VGG model [24] pre-trained on ImageNet [5] for the task of image classification<sup>1</sup>. For simplicity, we fine-tuned only the fully connected layers (fc6 and fc7) of each model while we preserved the pre-trained weights for the convolutional layers, which are shared among all the models of our system.

**Multi-Region CNN model.** Each of its region components inherits the fully connected layers of the VGG-Net and is finetuned separately from the others. To train them we follow the guidelines of R-CNN [10]. The 1000 channels classification layer of the ImageNet classification challenge[5] is replaced with a 21 channels classification layer for the 20 classes of PASCAL VOC detection challenge plus one for background. As an optimization objective we use the softmax-loss and the minimization is performed with stochastic gradient descent (SGD). The momentum is set to 0.9 and the learning rate is initially set to 0.001 and then reduced by a factor of 10 every 30k iterations. Our minibatch has 128 samples of which 25% are foreground samples and 75% are background samples. The positive samples are defined as the selective search proposals [26] that overlap with a ground-truth bounding box by at least 0.5. As negative samples we use the proposals that overlap with a ground-truth bounding box in the range [0.1, 0.5). The labelling of the training samples is relative to the original candidate boxes and is the same across all the different regions.

**Semantic segmentation-aware CNN.** The training is performed on two phases:

1. *Training of activation maps module:* We use as optimization objective a binary (foreground vs background) logistic loss applied on each spatial cell and for each class independently. The choice of having on each spatial cell a binary logistic loss per class instead of a softmax loss, was dictated by the fact that

<sup>1</sup><https://gist.github.com/ksimonyan/>

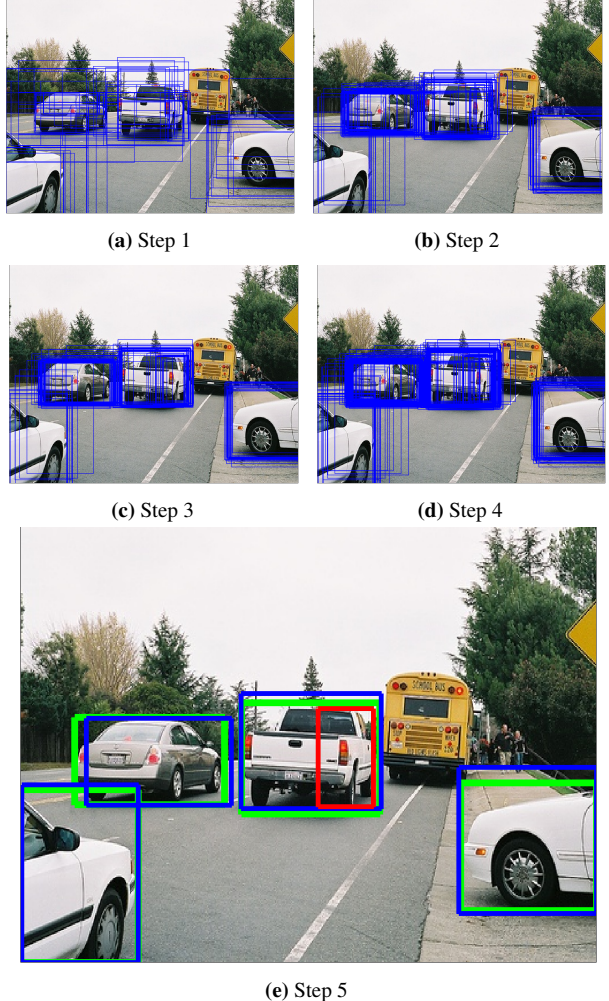


**Figure 6:** Illustration of the object localization scheme for instances of the class car. We describe the images from left to right and top to down order. **Step 1:** the initial box proposal of the image. For clarity we visualize only the box proposals that are not rejected after the first scoring step. **Step 2:** the new box locations obtained after performing CNN based bounding box regression on the boxes of Step 1. **Step 3:** the boxes obtained after a second step of box scoring and regressing on the boxes of Step 2. **Step 4:** the boxes of Step 2 and Step 3 merged together. **Step 5:** the detected boxes after applying non-maximum-suppression and box voting on the boxes of Step 4. On the final detections we use blue color for the true positives and red color for the false positives. Also, the ground truth bounding boxes are drawn with green color. The false positive that we see after the last step is a duplicate detection that survived from non-maximum-suppression.

the bounding box annotations of different classes for a given image are possible to overlap with each other. Thus, in contrast to the segmentation annotations typically provided on the semantic segmentation challenges, the labels of each cell on our artificially generated segmentation masks are not mutually exclusive

(see figure 5 middle column). For loss minimization we use SGD with minibatch of size 10. The momentum is set to 0.9 and the learning rate is initialized to 0.01 and decreased by a factor of 10 every 20 epochs. This procedure is followed for fine-tuning the FCN with the 4096 channels on  $fc_7$  and then is restarted for fine-tuning the FCN with the 512 channels on  $fc_7$ . For faster convergence during the second time, the learning rate of the randomly initialized  $fc_7$  layer (with the 512 channels) is multiplied by a factor of 10.

2. *Training of region adaptation module:* Here we follow the same procedure as for the region adaptation modules of the initial Multi-Region CNN model. During this phase, only the layers of the adaptation module are trained. The weights of the hidden fully connected layer are initialized randomly from a Gaussian distribution.

**Classification SVMs.** In order to train the SVMs we follow the same principles as in [10]. As positive samples are considered the ground truth bounding boxes and as negative samples are considered the selective search proposals [26] that overlap with the ground truth boxes by less than 0.3. We use hard negative mining the same way as in [10, 9].

**CNN-based bounding box regression.** To create this model we replaced the last classification layer of VGG-Net with a regression layer that outputs 4 channels per class. As a loss function we use the euclidean distance between the target values and the network predictions. For training samples we use the box proposals [26] that overlap by at least 0.4 with the ground truth bounding boxes. The target values of a training sample are defined the same way as in R-CNN [10] framework. The learning rate is initially set to 0.01 and reduced by a factor of 10 every 40k iterations. The momentum is set to 0.9 and the minibatch size is 128.

**Multi-Scale Implementation.** In our system we adopt a similar multi-scale implementation as in SPP-Net [12]. More specifically, we apply the activation maps modules of our models on multiple scales of an image and then a single scale is selected for each region adaptation module independently.

- *Multi-Region CNN model:* The activation maps module is applied on 7 scales of an image with their shorter dimension being in {480, 576, 688, 874, 1200, 1600, 2100}. For training, the region adaptation modules are applied on a random scale and for testing, a single scale is used such that the area of the scaled region is closest to  $224 \times 224$  pixels. In the case of rectangular ring regions, the scale is selected based on the area of the scaled outer box of the rectangular ring.

- *Semantic Segmentation-Aware CNN model:* The ac-

tivation maps module is applied on 3 scales of an image with their shorter dimension being in {576, 874, 1200}. For training, the region adaptation module is applied on a random scale and for testing, a single scale is selected such that the area of the scaled region is closest to  $288 \times 288$  pixels.

- *Bounding Box Regression CNN model:* The activation maps module is applied on 7 scales of an image with their shorter dimension being in {480, 576, 688, 874, 1200, 1600, 2100}. Both during training and testing, a single scale is used such that the area of the scaled region is closest to  $224 \times 224$  pixels.

## 6. Experimental Evaluation

We evaluate our detection system on PASCAL VOC2007 [7] and on PASCAL VOC2012 [8]. During the presentation of the results, we will use as baseline either the *Original candidate box* region alone (fig. 3a) and/or the R-CNN framework with VGG-Net [24]. We note that, when the *Original candidate box* region alone is used then the resulted model is a realization of the SPP-Net [12] object detection framework with the 16-layers VGG-Net [24]. For all the PASCAL VOC2007 results, we trained our models on the trainval set and tested them on the test set of the same year.

### 6.1. Results on PASCAL VOC2007

First, we asses the significance of each of the region adaptation modules alone on the object detection task. Results are reported in table 1. As we expected, the best performing component is the *Original candidate box*. What is surprising is the high detection performance of individual regions like the *Border Region* on figure 3i 54.8% or the *Contextual Region* on figure 3j 47.2%. Despite the fact that the area visible by them includes limited or not at all portion of the object, they outperform previous detection systems that were based on hand crafted features. Also interesting, is the high detection performance of the semantic segmentation aware region, 56.6%.

In table 2, we report the detection performance of our proposed modules. The Multi-Region CNN model without the semantic segmentation aware CNN features (*MR-CNN*), achieves 66.2% mAP, which is 4.2 points higher than *R-CNN with VGG-Net* (62.0%) and 4.5 points higher than the *Original candidate box* region alone (61.7%) (which as we said is a realization of the SPP-Net framework with the 16-layers VGG-Net). Moreover, its detection performance slightly exceeds that of *R-CNN with VGG-Net* and bounding box regression (66.0%). Extending the Multi-Region CNN model with the semantic segmentation aware CNN features (*MR-CNN & S-CNN*), boosts the performance of our recognition model another 1.3 points and reaches the

Adaptation Modules	areo	bike	bird	boat	bottle	bus	car	cat	chair	cow	table	dog	horse	mbike	person	plant	sheep	sofa	train	tv	mAP
<i>Original Box fig. 3a</i>	<b>0.729</b>	<b>0.715</b>	<b>0.593</b>	<b>0.478</b>	<b>0.405</b>	<b>0.713</b>	<b>0.725</b>	<b>0.741</b>	<b>0.418</b>	<b>0.694</b>	0.591	<b>0.713</b>	0.662	<b>0.725</b>	<b>0.560</b>	<b>0.312</b>	<b>0.601</b>	0.565	0.669	<b>0.731</b>	<b>0.617</b>
<i>Left Half Box fig. 3b</i>	0.635	0.659	0.455	0.364	0.322	0.621	0.640	0.589	0.314	0.620	0.463	0.573	0.545	0.641	0.477	0.300	0.532	0.442	0.546	0.621	0.518
<i>Right Half Box fig. 3c</i>	0.626	0.605	0.470	0.331	0.314	0.607	0.616	0.641	0.278	0.487	0.513	0.548	0.564	0.585	0.459	0.262	0.469	0.465	0.573	0.620	0.502
<i>Up Half Box fig. 3d</i>	0.591	0.651	0.470	0.266	0.361	0.629	0.656	0.641	0.305	0.604	0.511	0.604	0.643	0.588	0.466	0.220	0.545	0.528	0.590	0.570	0.522
<i>Bottom Half Box fig. 3e</i>	0.607	0.631	0.406	0.397	0.233	0.594	0.626	0.559	0.285	0.417	0.404	0.520	0.490	0.649	0.387	0.233	0.457	0.344	0.566	0.617	0.471
<i>Central Region fig. 3f</i>	0.552	0.622	0.413	0.244	0.283	0.502	0.594	0.603	0.282	0.523	0.424	0.516	0.495	0.584	0.386	0.232	0.527	0.358	0.533	0.587	0.463
<i>Central Region fig. 3g</i>	0.674	0.705	0.547	0.367	0.337	0.678	0.698	0.687	0.381	0.630	0.538	0.659	0.667	0.679	0.507	0.309	0.557	0.530	0.611	0.694	0.573
<i>Border Region fig. 3h</i>	0.694	0.696	0.552	0.470	0.389	0.687	0.706	0.703	0.398	0.631	0.515	0.660	0.643	0.686	0.539	0.307	0.582	0.537	0.618	0.717	0.586
<i>Border Region fig. 3i</i>	0.651	0.649	0.504	0.407	0.333	0.670	0.704	0.624	0.323	0.625	0.533	0.594	0.656	0.627	0.517	0.223	0.533	0.515	0.604	0.663	0.548
<i>Contextual Region fig. 3j</i>	0.624	0.568	0.425	0.380	0.255	0.609	0.650	0.545	0.222	0.509	0.522	0.427	0.563	0.541	0.431	0.163	0.482	0.392	0.597	0.532	0.472
<i>Semantic-aware region.</i>	0.652	0.684	0.549	0.407	0.225	0.658	0.676	0.738	0.316	0.596	<b>0.635</b>	0.705	<b>0.670</b>	0.689	0.545	0.230	0.522	<b>0.598</b>	<b>0.680</b>	0.548	0.566

**Table 1:** Detection performance of individual region adaptation modules. Results on VOC 2007 test set.

Approach	areo	bike	bird	boat	bottle	bus	car	cat	chair	cow	table	dog	horse	mbike	person	plant	sheep	sofa	train	tv	mAP
<i>R-CNN with VGG-Net</i>	0.716	0.735	0.581	0.422	0.394	0.707	0.760	0.745	0.387	0.710	0.569	0.745	0.679	0.696	0.593	0.357	0.621	0.640	0.665	0.712	0.622
<i>R-CNN with VGG-Net &amp; bbox reg.</i>	0.734	0.770	0.634	0.454	0.446	0.751	0.781	0.798	0.405	0.737	0.622	0.794	0.781	0.731	0.642	0.356	0.668	0.672	0.704	0.711	0.660
<i>Best approach of [28]</i>	0.725	0.788	0.67	0.452	0.510	0.738	0.787	0.783	0.467	0.738	0.615	0.771	0.764	0.739	0.665	0.392	0.697	0.594	0.668	0.729	0.665
<i>Best approach of [28] &amp; bbox reg.</i>	0.741	<b>0.832</b>	0.670	0.508	0.516	0.762	0.814	0.772	0.481	0.789	0.656	0.773	0.784	0.751	0.701	0.414	0.696	0.608	0.702	0.737	0.685
<i>Original Box fig. 3a</i>	0.729	0.715	0.593	0.478	0.405	0.713	0.725	0.741	0.418	0.694	0.591	0.713	0.662	<b>0.725</b>	0.560	0.312	0.601	0.565	0.669	0.731	0.617
<i>MR-CNN</i>	0.749	0.757	0.645	0.549	0.447	0.741	0.755	0.760	0.481	0.724	0.764	0.765	0.724	0.749	0.617	0.348	0.617	0.640	0.735	0.760	0.662
<i>MR-CNN &amp; S-CNN</i>	0.768	0.757	0.676	0.551	0.456	0.776	0.765	0.784	0.467	0.747	0.688	0.793	0.742	0.770	0.625	0.374	0.643	0.638	0.740	0.747	0.675
<i>MR-CNN &amp; S-CNN &amp; Loc. scheme</i>	<b>0.787</b>	0.818	<b>0.767</b>	<b>0.666</b>	<b>0.618</b>	<b>0.817</b>	<b>0.853</b>	<b>0.827</b>	<b>0.570</b>	<b>0.819</b>	<b>0.732</b>	<b>0.846</b>	<b>0.860</b>	<b>0.805</b>	<b>0.749</b>	<b>0.449</b>	<b>0.717</b>	<b>0.697</b>	<b>0.787</b>	<b>0.799</b>	<b>0.749</b>

**Table 2:** Detection performance of our modules. Results on VOC 2007 test set.

Approach	areo	bike	bird	boat	bottle	bus	car	cat	chair	cow	table	dog	horse	mbike	person	plant	sheep	sofa	train	tv	mAP
<i>R-CNN with VGG-Net from [28]</i>	0.402	0.433	0.234	0.144	0.133	0.482	0.445	0.364	0.171	0.340	0.279	0.363	0.268	0.282	0.212	0.103	0.337	0.366	0.316	0.489	0.308
<i>Best approach of [28]</i>	0.463	0.581	0.311	0.216	0.258	0.571	0.582	0.435	0.230	0.464	0.290	0.407	0.406	0.463	0.334	0.106	0.413	0.409	0.458	0.563	0.398
<i>Best approach of [28] &amp; bbox reg.</i>	0.471	<b>0.618</b>	0.352	0.181	0.297	<b>0.660</b>	0.647	0.480	<b>0.253</b>	0.504	0.349	0.437	0.508	0.494	0.368	0.137	0.447	0.436	0.498	<b>0.605</b>	0.437
<i>Original Candidate Box</i>	0.449	0.426	0.237	0.175	0.157	0.441	0.444	0.377	0.182	0.295	0.303	0.312	0.249	0.332	0.187	0.099	0.302	0.286	0.337	0.499	0.305
<i>MR-CNN</i>	0.495	0.505	0.292	0.235	0.179	0.513	0.504	0.481	0.206	0.381	0.375	0.387	0.296	0.403	0.239	0.151	0.341	0.389	0.422	0.521	0.366
<i>MR-CNN &amp; S-CNN</i>	0.507	0.523	0.316	0.266	0.177	0.547	0.513	0.492	0.210	0.450	0.361	0.433	0.309	0.408	0.246	0.151	0.359	0.427	0.438	0.534	0.383
<i>MR-CNN &amp; S-CNN &amp; Loc. scheme</i>	<b>0.549</b>	0.613	<b>0.430</b>	<b>0.315</b>	<b>0.383</b>	0.646	<b>0.650</b>	<b>0.512</b>	<b>0.253</b>	<b>0.544</b>	<b>0.505</b>	<b>0.521</b>	<b>0.591</b>	<b>0.540</b>	<b>0.393</b>	<b>0.159</b>	<b>0.485</b>	<b>0.468</b>	<b>0.553</b>	0.573	<b>0.484</b>

**Table 3:** Detection performance of our modules for IoU > 0.7. Results on VOC 2007 test set.

total of 67.5% mAP. Comparing to the recently published method of Yuting et al. [28], our *MR-CNN & S-CNN* model scores 1 point higher than their best performing method that includes generation of extra box proposals via Bayesian optimization and structured loss during the fine-tuning of the VGG-Net. Significant is also the improvement that we get when we couple our recognition model with the CNN model for bounding box regression under the iterative scheme proposed (*MR-CNN & S-CNN & Loc. scheme*). Specifically, the detection performance is raised from 67.5% to 74.9% setting the new state-of-the-art on this dataset.

In table 3, we report the detection performance of our system when the threshold for considering a detection positive is set to 0.7. This metric was proposed from [28] in order to reveal the localization capability of their method. From the table we observe that each of our modules exhibit very good localization capability, which was our goal when designing them, and our overall system exceeds in that metric the approach of [28].

## 6.2. Detection error analysis

We use the tool of Hoiem et al. [15] to analyse the detection errors of our system. In figure 8, we plot pie charts

with the percentage of detections that are false positive due to bad localization, confusion with similar category, confusion with other category, and triggered on the background or an unlabelled object. In the first row is our baseline which is the *Original candidate box* only model. This model is actually a realization of the SPP-Net framework with the 16-layers VGG-Net. In the middle row is the Multi-Region CNN model without the semantic segmentation aware CNN features and in the bottom row is our overall system that includes the Multi-Region CNN model with the semantic segmentation aware CNN features coupled with the CNN-based bounding box regression under the iterative localization scheme. We plot only the pie charts for the classes boat, bottle, chair, and pottedplant because of space limitations and the fact that they are the most difficult categories of the PASCAL VOC challenge.

We see from the pie charts that, by using the Multi-Region CNN model, a considerable reduction in the percentage of false positives due to bad localization is achieved. This validates our argument that focusing on multiple regions of an object increases the localization sensitivity of our model. Furthermore, when our recognition model is integrated on the localization module developed for it, the

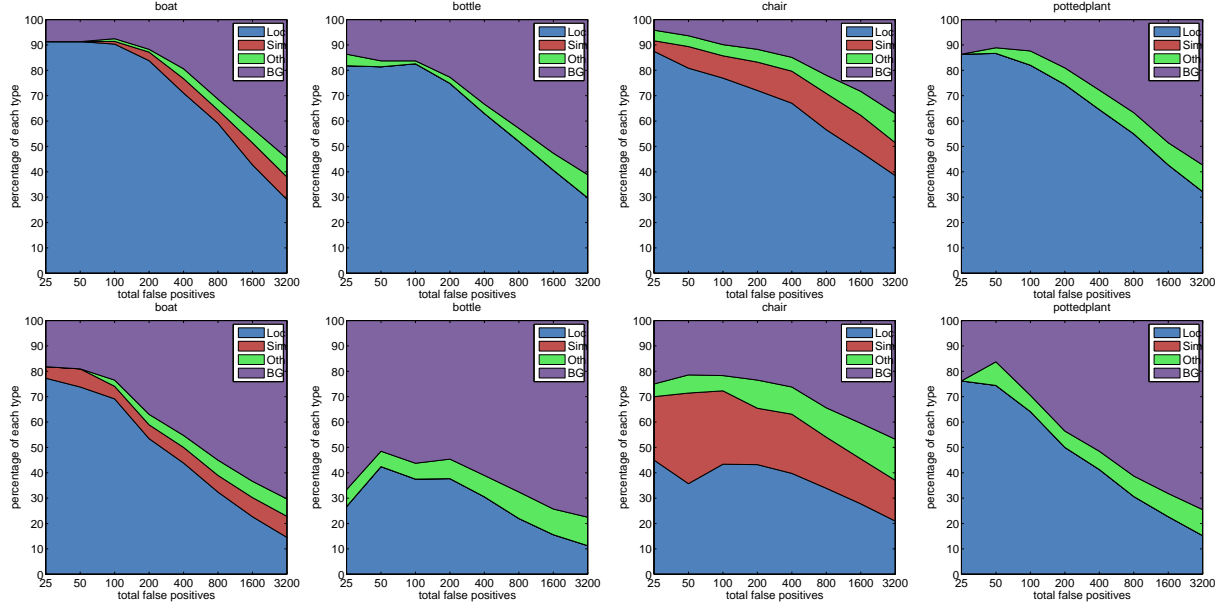


**Figure 7:** Top ranked false positive types. **Top row:** our baseline which is the *original candidate box* only model. This model is actually a realization of the SPP-Net framework with the 16-layers VGG-Net. **Bottom row:** our overall system that includes the Multi-Region CNN model with the semantic segmentation aware CNN features coupled with the CNN-based bounding box regression under the iterative localization scheme. We plot only the graphs for the classes boat, bottle, chair, and pottedplant because of space limitations and the fact that they are the most difficult categories of PASCAL VOC challenge.

Approach	areo	bike	bird	boat	bottle	bus	car	cat	chair	cow	table	dog	horse	mbike	person	plant	sheep	sofa	train	tv
<i>Original candidate box-Baseline</i>	0.7543	0.7325	0.6634	0.5816	0.5775	0.7109	0.7390	0.7277	0.5718	0.7112	0.6007	0.7000	0.7039	0.7194	0.6607	0.5339	0.6855	0.6461	0.6903	0.7359
<i>MR-CNN</i>	0.7938	0.7864	0.7180	0.6424	0.6222	0.7609	0.7918	0.7758	0.6186	0.7483	0.6802	0.7448	0.7562	0.7569	0.7166	0.5753	0.7268	0.7148	0.7391	0.7556

**Table 4:** Correlation between the IoU overlap of selective search box proposals [26] (with the closest ground truth bounding box) and the score assigned to them.

Approach	areo	bike	bird	boat	bottle	bus	car	cat	chair	cow	table	dog	horse	mbike	person	plant	sheep	sofa	train	tv
<i>Original candidate box-Baseline</i>	0.9327	0.9324	0.9089	0.8594	0.8570	0.9389	0.9455	0.9250	0.8603	0.9237	0.8806	0.9209	0.9263	0.9317	0.9151	0.8415	0.8932	0.9060	0.9241	0.9125
<i>MR-CNN</i>	0.9462	0.9479	0.9282	0.8843	0.8740	0.9498	0.9593	0.9355	0.8790	0.9338	0.9127	0.9358	0.9393	0.9440	0.9341	0.8607	0.9120	0.9314	0.9413	0.9210

**Table 5:** The Area-Under-Curve (AUC) measure for the well-localized box proposals against the mis-localized box proposals.

reduction of false positives due to bad localization is huge. A similar observation can be deducted from figure 7 where we plot the top-ranked false positive types of the baseline and of our overall proposed system.

### 6.3. Localization awareness of Multi-Region CNN model

Two extra experiments are presented here that indicate the localization awareness of our Multi-Region CNN model without the semantic segmentation aware CNN features (*MR-CNN*) against the model that uses only the original candidate box (*Baseline*).

**Correlation between the scores and the IoU overlap of box proposals.** In this experiment, we estimate the correlation between the IoU overlap of box proposals [26] (with the closest ground truth bounding box) and the score assigned to them from the two examined models. High correlation coefficient means that better localized box proposals will

tend to be scored higher than mis-localized ones. We report the correlation coefficients of the aforementioned quantities both for the *Baseline* and *MR-CNN* models in table 4. Because with this experiment we want to emphasize on the localization aspect of the Multi-Region CNN model, we use proposals that overlap with the ground truth bounding boxes by at least 0.1 IoU.

**Area-Under-the-Curve of well-localized proposals against mis-localized proposals.** The ROC curves are typically used to illustrate the capability of a classifier to distinguish between two classes. This discrimination capability can be measured by computing the Area-Under-the-Curve (AUC) metric. The higher the AUC measure is, the more discriminative is the classifier between the two classes. In our case, the set of well-localized box proposals is the positive class and the set of mis-localized box proposals is the negative class. As well-localized are considered the box proposals that overlap with a ground-truth

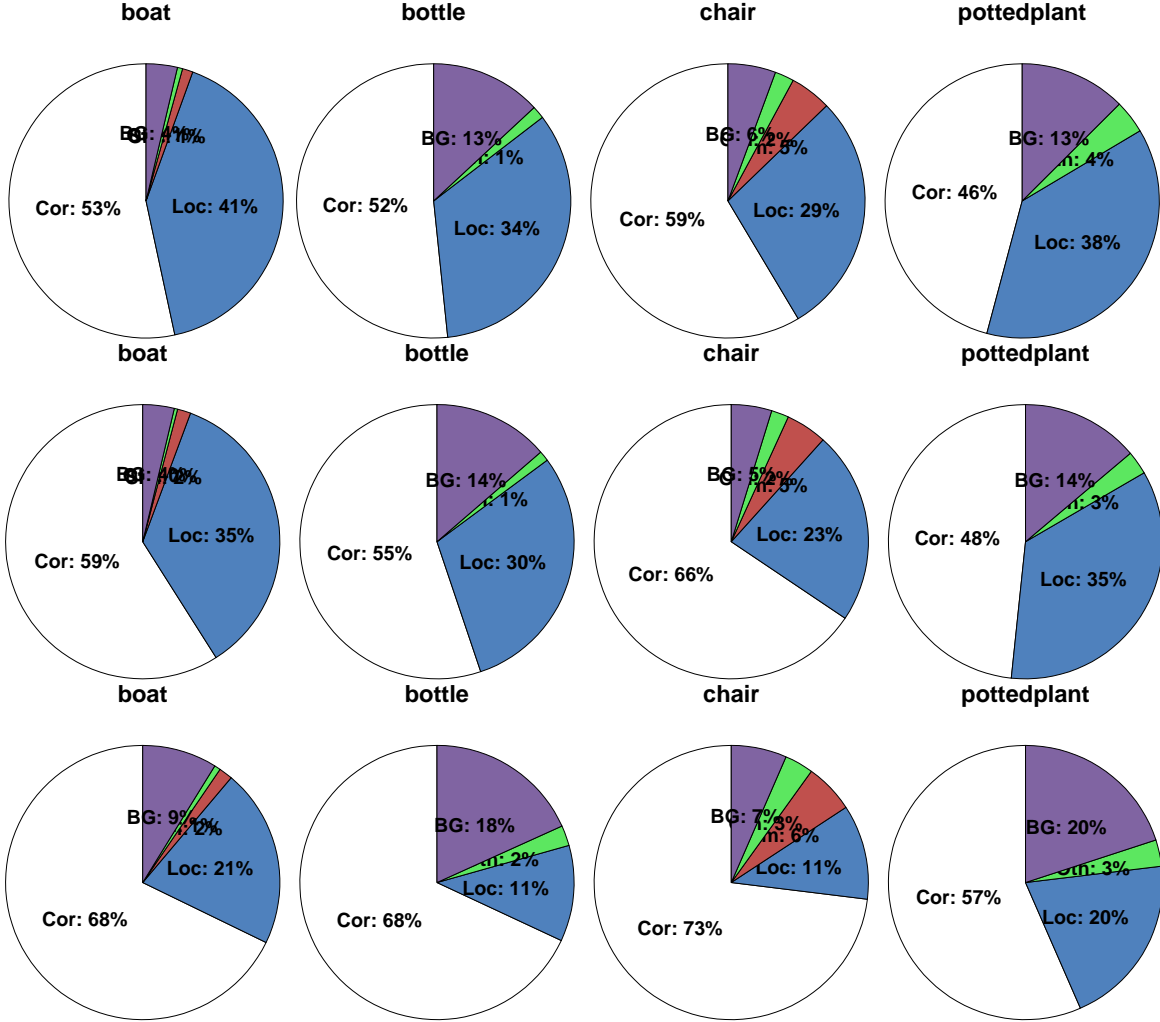


**Figure 8:** Fraction of top N detections (N=num of objs in category) that are correct (Cor), or false positives due to poor localization (Loc), confusion with similar objects (Sim), confusion with other VOC objects (Oth), or confusion with background or unlabelled objects (BG). **Top row:** our baseline which is the *original candidate box* only model. This model is actually a realization of the SPP-Net framework with the 16-layers VGG-Net. **Middle row:** Multi-Region CNN model without the semantic segmentation aware CNN features. **Bottom row:** our overall system that includes the Multi-Region CNN model with the semantic segmentation aware CNN features coupled with the CNN-based bounding box regression under the iterative localization scheme. We plot only the pie charts for the classes boat, bottle, chair, and pottedplant because of space limitations and the fact that they are the most difficult categories of PASCAL VOC challenge.

bounding box in the range [0.5, 1.0] and as mis-localized are considered the box proposals that overlap with a ground truth bounding box in the range [0.1, 0.5]. In table 5, we report the AUC measure for each class separately and both for the *MR-CNN* and the *Baseline* models.

#### 6.4. Results on PASCAL VOC2012

In table 6, we compare the detection system proposed by us against other published work on the test set of PASCAL VOC2012 [8]. Specifically, our detection system involves the Multi-Region CNN model enriched with the semantic segmentation aware CNN features and coupled with the CNN based bounding box regression under the iterative

localization scheme. We tested two instances of our system. Both of them have exactly the same components but they have been trained on different datasets. For the first one, the fine-tuning of the networks as well as the training of the detection SVMs was performed on VOC2007 trainval dataset that includes 5011 annotated images. With this model (*Ours – VOC2007 trainval trained model*), the mAP achieved on VOC2012 test set is 69.1%. For the second one, the fine-tuning of the networks was performed on VOC2012 train dataset that includes 5717 annotated images and the training of the detection SVMs was performed on VOC2012 trainval dataset that includes 11540 annotated images. Using this model (*Ours – VOC2012 trainval trained model*),

Approach	areo	bike	bird	boat	bottle	bus	car	cat	chair	cow	table	dog	horse	mbike	person	plant	sheep	sofa	train	tv	mAP
<i>R-CNN</i> [ <a href="#">10</a> ] with VGG-Net & bbox reg.	0.792	0.723	0.629	0.437	0.451	0.677	0.667	0.830	0.393	0.662	0.517	0.822	0.732	0.765	0.642	0.337	0.667	0.561	0.683	0.610	0.630
<i>Network In Network</i> [ <a href="#">19</a> ]	0.802	0.738	0.619	0.437	0.430	0.703	0.676	0.807	0.419	0.697	0.517	0.782	0.752	0.769	0.651	0.386	0.683	0.580	0.687	0.633	0.638
<i>Best approach of</i> [ <a href="#">28</a> ] <i>bbox reg.</i>	0.829	0.761	0.641	0.446	0.494	0.703	0.712	<b>0.846</b>	0.427	0.686	0.558	0.827	0.771	0.799	0.687	0.414	<b>0.690</b>	0.600	0.720	0.662	0.664
<i>Ours – VOC2007 trainval trained model</i>	0.829	0.789	0.708	0.528	0.555	0.737	0.738	0.843	0.480	0.702	0.571	0.845	0.769	<b>0.819</b>	0.755	<b>0.426</b>	0.685	0.599	0.728	0.717	0.691
<i>Ours – VOC2012 trainval trained model</i>	<b>0.850</b>	<b>0.796</b>	<b>0.715</b>	<b>0.553</b>	<b>0.577</b>	<b>0.760</b>	<b>0.739</b>	<b>0.846</b>	<b>0.505</b>	<b>0.743</b>	<b>0.617</b>	<b>0.855</b>	<b>0.799</b>	0.817	<b>0.764</b>	0.410	<b>0.690</b>	<b>0.612</b>	<b>0.777</b>	<b>0.721</b>	<b>0.707</b>

**Table 6:** Comparative results on VOC 2012 test set.

the mAP is raised from 69.1% to 70.7%. Both of the obtained detection performances exceed any other published work and set the new state-of-the-art on this dataset.

## 7. Qualitative Results

In figures 12 - 14 we present some object detections obtained by our approach. We use blue bounding boxes to mark the true positive detections and red bounding boxes to mark the false positive detections. The ground truth bounding boxes are marked with green color.

**Failure cases.** Accurately detecting multiple adjacent object instances remains in many cases a difficult problem even for our approach. In figure 9 we present a few difficult examples of this type. In figure 10 we show some other failure cases.

**Missing annotations.** There were also cases of object instances that were correctly detected by our approach but which were not in the ground truth annotation of PASCAL VOC2007. Figure 11 presents a few such examples of non-annotated object instances.

## 8. Conclusions

We proposed a powerful CNN-based representation for object detection that relies on two key factors: (i) diversification of the discriminative appearance factors captured by it through steering its focus on different regions of the object, and (ii) the encoding of semantic segmentation-aware features. By using it in the context of a CNN-based localization refinement scheme, we show that it achieves excellent results that surpass the state-of-the art by a significant margin.

## References

- [1] P. Arbeláez, J. Pont-Tuset, J. Barron, F. Marques, and J. Malik. Multiscale combinatorial grouping. In *Computer Vision and Pattern Recognition*, 2014. [2](#)
- [2] Y. Bengio, P. Lamblin, D. Popovici, H. Larochelle, et al. Greedy layer-wise training of deep networks. *Advances in neural information processing systems*, 19:153, 2007. [1](#)
- [3] J. Dai, K. He, and J. Sun. Convolutional feature masking for joint object and stuff segmentation. *arXiv preprint arXiv:1412.1283*, 2014. [2](#)
- [4] N. Dalal and B. Triggs. Histograms of oriented gradients for human detection. In *Computer Vision and Pattern Recognition*, 2005. [1](#)
- [5] J. Deng, W. Dong, R. Socher, L.-J. Li, K. Li, and L. Fei-Fei. Imagenet: A large-scale hierarchical image database. In *Computer Vision and Pattern Recognition, 2009. CVPR 2009. IEEE Conference on*, pages 248–255. IEEE, 2009. [7](#)
- [6] J. Dong, Q. Chen, S. Yan, and A. Yuille. Towards unified object detection and semantic segmentation. In *Computer Vision–ECCV 2014*, pages 299–314. Springer, 2014. [4](#)
- [7] M. Everingham, L. Van Gool, C. Williams, J. Winn, and A. Zisserman. The pascal visual object classes challenge 2007 (voc 2007) results (2007), 2008. [2, 4, 8](#)
- [8] M. Everingham, L. Van Gool, C. Williams, J. Winn, and A. Zisserman. The pascal visual object classes challenge 2012, 2012. [2, 8, 11](#)
- [9] P. F. Felzenszwalb, R. B. Girshick, D. McAllester, and D. Ramanan. Object detection with discriminatively trained part-based models. *Pattern Analysis and Machine Intelligence, IEEE Transactions on*, 32(9):1627–1645, 2010. [1, 8](#)
- [10] R. Girshick, J. Donahue, T. Darrell, and J. Malik. Rich feature hierarchies for accurate object detection and semantic segmentation. In *Computer Vision and Pattern Recognition (CVPR), 2014 IEEE Conference on*, pages 580–587. IEEE, 2014. [1, 2, 3, 7, 8, 12](#)
- [11] B. Hariharan, P. Arbeláez, R. Girshick, and J. Malik. Simultaneous detection and segmentation. In *Computer Vision–ECCV 2014*, pages 297–312. Springer, 2014. [4](#)
- [12] K. He, X. Zhang, S. Ren, and J. Sun. Spatial pyramid pooling in deep convolutional networks for visual recognition. *arXiv preprint arXiv:1406.4729*, 2014. [2, 3, 8](#)
- [13] K. He, X. Zhang, S. Ren, and J. Sun. Delving deep into rectifiers: Surpassing human-level performance on imagenet classification. *arXiv preprint arXiv:1502.01852*, 2015. [2](#)
- [14] G. E. Hinton and R. R. Salakhutdinov. Reducing the dimensionality of data with neural networks. *Science*, 313(5786):504–507, 2006. [1](#)
- [15] D. Hoiem, Y. Chodpathumwan, and Q. Dai. Diagnosing error in object detectors. In *Computer Vision–ECCV 2012*, pages 340–353. Springer, 2012. [9](#)
- [16] S. Ioffe and C. Szegedy. Batch normalization: Accelerating deep network training by reducing internal covariate shift. *arXiv preprint arXiv:1502.03167*, 2015. [2](#)
- [17] A. Krizhevsky, I. Sutskever, and G. E. Hinton. Imagenet classification with deep convolutional neural networks. In *Advances in neural information processing systems*, pages 1097–1105, 2012. [1, 2](#)
- [18] Y. LeCun, B. Boser, J. S. Denker, D. Henderson, R. E. Howard, W. Hubbard, and L. D. Jackel. Backpropagation applied to handwritten zip code recognition. *Neural computation*, 1(4):541–551, 1989. [1](#)

[19] M. Lin, Q. Chen, and S. Yan. Network in network. *CoRR*, abs/1312.4400, 2013. [12](#)

[20] J. Long, E. Shelhamer, and T. Darrell. Fully convolutional networks for semantic segmentation. *arXiv preprint arXiv:1411.4038*, 2014. [5](#)

[21] D. G. Lowe. Distinctive image features from scale-invariant keypoints. *International journal of computer vision*, 60(2):91–110, 2004. [1](#)

[22] R. Mottaghi, X. Chen, X. Liu, N.-G. Cho, S.-W. Lee, S. Fidler, R. Urtasun, and A. Yuille. The role of context for object detection and semantic segmentation in the wild. In *Computer Vision and Pattern Recognition (CVPR), 2014 IEEE Conference on*, pages 891–898. IEEE, 2014. [4](#)

[23] P. Sermanet, D. Eigen, X. Zhang, M. Mathieu, R. Fergus, and Y. LeCun. Overfeat: Integrated recognition, localization and detection using convolutional networks. *arXiv preprint arXiv:1312.6229*, 2013. [1](#)

[24] K. Simonyan and A. Zisserman. Very deep convolutional networks for large-scale image recognition. *arXiv preprint arXiv:1409.1556*, 2014. [1, 2, 3, 5, 7, 8](#)

[25] C. Szegedy, W. Liu, Y. Jia, P. Sermanet, S. Reed, D. Anguelov, D. Erhan, V. Vanhoucke, and A. Rabinovich. Going deeper with convolutions. *arXiv preprint arXiv:1409.4842*, 2014. [2](#)

[26] K. E. Van de Sande, J. R. Uijlings, T. Gevers, and A. W. Smeulders. Segmentation as selective search for object recognition. In *Computer Vision (ICCV), 2011 IEEE International Conference on*, pages 1879–1886. IEEE, 2011. [1, 2, 6, 7, 8, 10](#)

[27] A. Vedaldi, V. Gulshan, M. Varma, and A. Zisserman. Multiple kernels for object detection. In *Computer Vision, 2009 IEEE 12th International Conference on*, pages 606–613. IEEE, 2009. [1](#)

[28] Z. Yuting, S. Kihyuk, V. Ruben, P. Gang, and H. Lee. Improving object detection with deep convolutional networks via bayesian optimization and structured prediction. *arXiv preprint arXiv:1504.03293*, 2015. [9, 12](#)

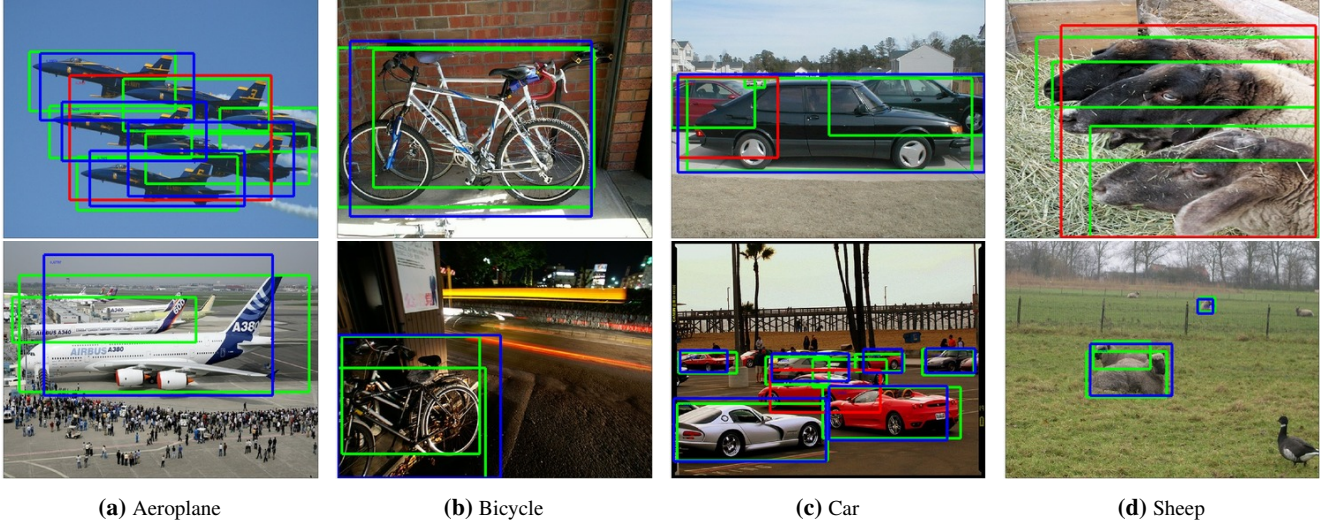


**Figure 9:** Examples of multiple adjacent object instances where our approach fails to detect all of them. We use blue bounding boxes to mark the true positive detections and red bounding boxes to mark the false positive detections. The ground truth bounding boxes are drawn with green color.



**Figure 10:** Examples of false positive detections for the class boat due to the fact that the detected bounding boxes do not include inside their borders the mast of the boat (it is worth noting that on some cases also the annotation provided from PASCAL neglects to include them on its ground truth bounding boxes). The false positive bounding boxes are drawn with red color and the ground truth bounding boxes are drawn with green color.

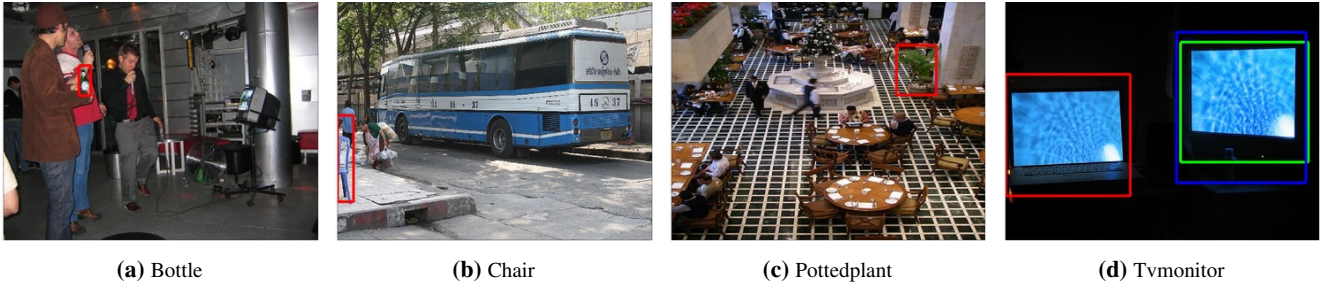
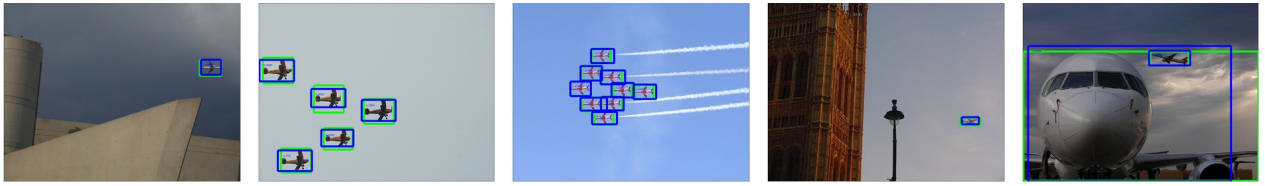


**Figure 11 – Missing Annotations:** Examples where our proposed detection system has truly detected an object instance, but because of missed annotations it is considered false positive. For those detections we used red bounding boxes. For any true positive detection on those images we use blue bounding boxes and the corresponding ground truth bounding boxes are drawn with green color.



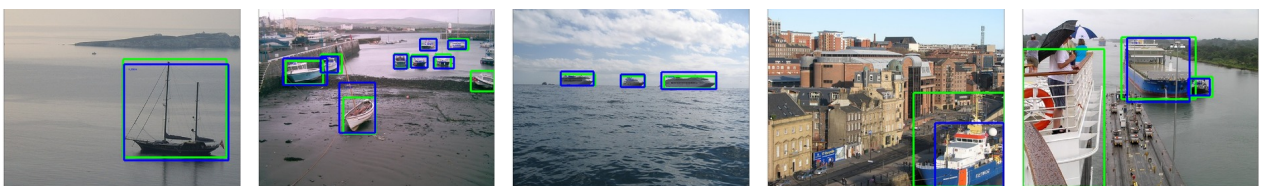
(a) Aeroplane detections.



(b) Bicycle detections.



(c) Bird detections.



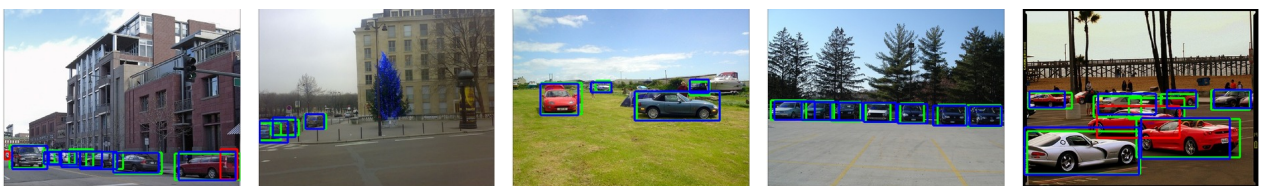
(d) Boat detections.



(e) Bottle detections.

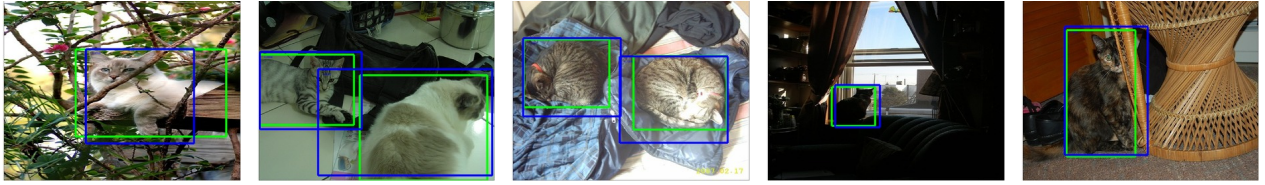


(f) Bus detections.



(g) Car detections.

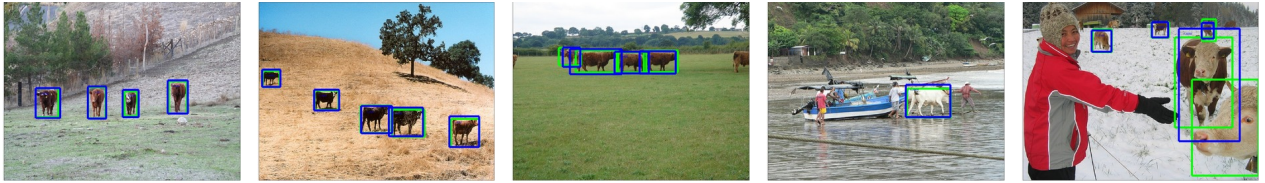
**Figure 12:** We use blue bounding boxes to mark the true positive detections and red bounding boxes (if any) to mark the false positive detections. The ground truth bounding boxes are marked with green color.



(a) Cat detections.



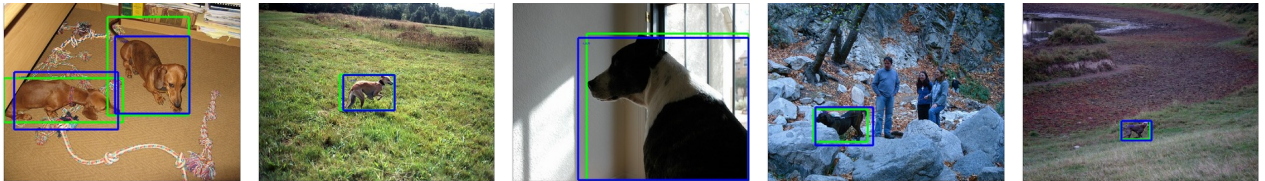
(b) Chair detections.



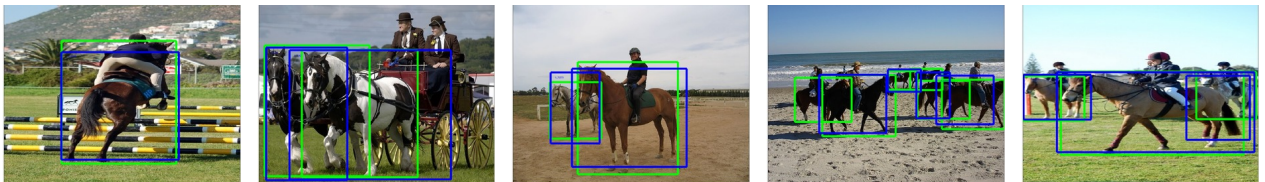
(c) Cow detections.



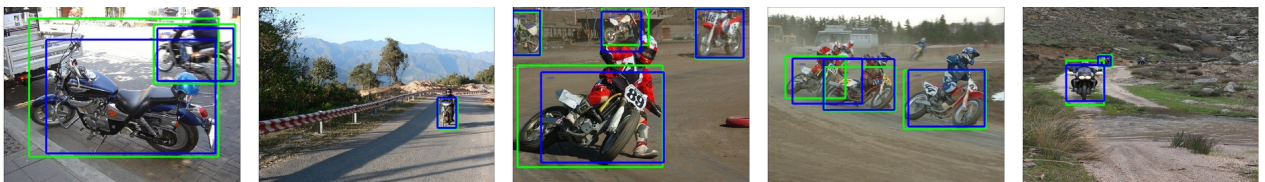
(d) Diningtable detections.



(e) Dog detections.



(f) Horse detections.

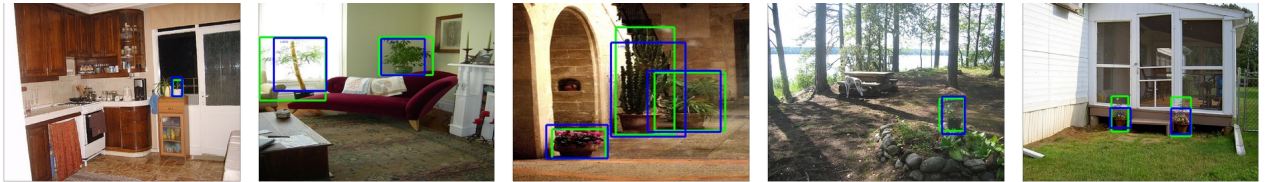


(g) Motorbike detections.

**Figure 13:** We use blue bounding boxes to mark the true positive detections and red bounding boxes (if any) to mark the false positive detections. The ground truth bounding boxes are marked with green color.



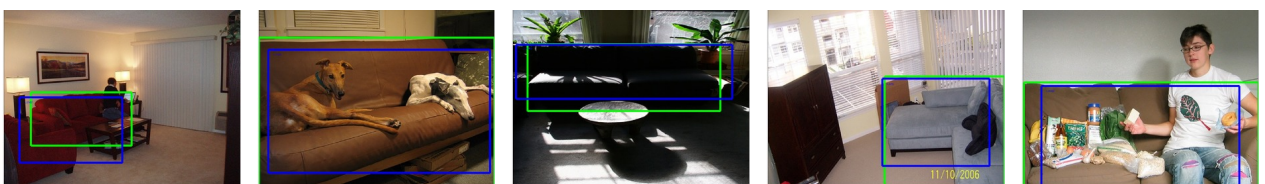
(a) Person detections.



(b) Pottedplant detections.



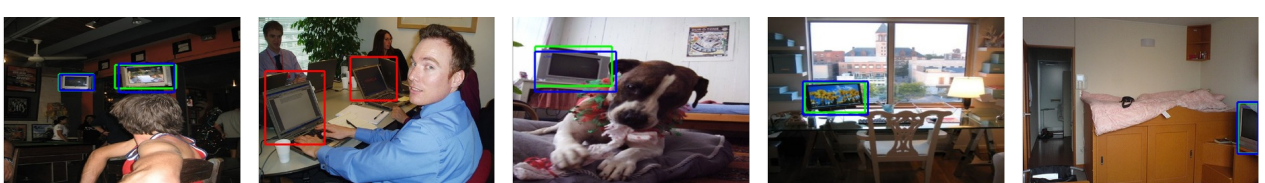
(c) Sheep detection.



(d) Sofa detections.



(e) Train detections.



(f) Tvmonitor detections.

**Figure 14:** We use blue bounding boxes to mark the true positive detections and red bounding boxes (if any) to mark the false positive detections. The ground truth bounding boxes are marked with green color.